A Trifector of New Insights into Ovine Footrot for Infection Drivers, Immune Response and Host Pathogen Interactions.

Adam M. Blanchard[1*], Ceri E. Staley[1], Laurence Shaw[2], Sean R Wattegedera[3], Christina-Marie Baumbach[4], Jule K. Michler[4], Catrin Rutland[1], Charlotte Back[1], Nerissa Newbold[1±], Gary Entrican[3#], Sabine Tötemeyer[1*]

[*]Corresponding authors

[1]School of Veterinary Medicine and Science, University of Nottingham, Sutton Bonington, Loughborough, Leicestershire, LE12 5RD.

[2]School of Science and Technology, Nottingham Trent University, Nottingham, NG11 8NS

[3]Moredun Research Institute, Pentlands Science Park, Bush Loan, Penicuik, Midlothian, Scotland, EH26 0PZ.

[4]Institute of Anatomy, Histology and Embryology, Faculty of Veterinary Medicine, Leipzig University, Leipzig, Germany

Current addresses:

[±]Bristol Veterinary School, University of Bristol, Langford House, Langford, Somerset, BS40 5DU

[#]The Roslin Institute, The University of Edinburgh, Easter Bush, Scotland, EH25 9RG

Abstract

Footrot is a polymicrobial infectious disease in sheep causing severe lameness, leading to one of the industry's biggest welfare problems. The complex aetiology of footrot makes in-situ or in-vitro investigations difficult. Computational methods offer a solution to understanding the bacteria involved, how they may interact with the host and ultimately providing a way to identify targets for future hypotheses driven investigative work. Here we present the first combined global analysis of the bacterial community transcripts together with the host immune response in healthy and diseased ovine feet during a natural polymicrobial infection state using metatranscriptomics. The intra tissue and surface bacterial populations and the most abundant bacterial transcriptome were analysed, demonstrating footrot affected skin has a reduced diversity and increased abundances of, not only the causative bacteria *Dichelobacter nodosus*, but other species such as *Mycoplasma fermentans* and *Porphyromonas asaccharolytica*. Host transcriptomics reveals a suppression of biological processes relating to skin barrier function, vascular functions, and immunosurveillance in unhealthy interdigital skin, supported by histological findings that type I collagen (associated with scar tissue formation) is significantly increased in footrot affected interdigital skin comparted to outwardly healthy skin. Finally, we provide some interesting indications of host and pathogen interactions associated with virulence genes and the host spliceosome which could lead to the identification of future therapeutic targets.

Impact Statement

Lameness in sheep is a global welfare and economic concern and footrot is the leading cause of lameness, affecting up to 70% of flocks in the U.K. Current methods

for control of this disease are labour intensive and account for approximately 65% of antibiotic use in sheep farming, whilst preventative vaccines suffer from poor efficacy due to antigen competition. Our limited understanding of cofounders, such as strain variation and polymicrobial nature of infection mean new efficacious, affordable and scalable control measures are not receiving much attention. Here we examine the surface and intracellular bacterial populations and propose potential interactions with the host. Identification of these key bacterial species involved in the initiation and progression of disease and the host immune mechanisms could help form the basis of new therapies.

Introduction

Ovine footrot is a persistent animal welfare issue and has a significant financial burden for farmers due to the cost of preventative footbaths, antibiotic treatments, and reduced carcass weights at slaughter (1). The causative bacterium *Dichelobacter nodosus* (*D. nodosus*) has received extensive attention since its description in the initiation of footrot (2). However, it has been accepted since the beginning of the 20th century that footrot is a polymicrobial disease, with *Fusobacterium necrophorum (F. necrophorum)*, *Spirochaeta penortha (S. penortha)* (3), *Treponema podovis (T. podovis)* (4) and *Corynebacterium pyogenes (C. pyogenes)* (5) proposed as species that can exacerbate the lesions.

Currently our understanding of bacterial populations associated with footrot is only based on 16S rRNA analysis from the skin surface (6, 7). The highly abundant genera identified in the footrot samples were congruent with those identified previously by standard microbiological techniques (*Corynebacterium, Fusobacterium,*

Dichelobacter and *Treponema*). However, additional genera were also identified (*Mycoplasma, Psychrobacter* and *Porphyromonas*) (7) and their absence using traditional culture techniques, could be due to the fastidious nature of the bacteria (8) or that they were not yet identified (9). Investigating the total bacterial load within tissues, we have shown recently, that in healthy tissues, bacterial load is similar throughout tissue depth and did not extend beyond the follicular depth in the reticular dermis. In contrast, in footrot samples, the bacterial load was highest in the superficial (or cornified) epidermal layers and decreasing in the deeper layers but still beyond follicular depth (10). This suggests that the infection allows for further invasion from other species of bacteria to penetrate deeper into the interdigital tissue, however these data were limited to presence of bacteria based on universal primers not allowing to identify species.

There is also a lack of information regarding the host infection, how an immune response is mounted and the species interactions. This area of investigation has recently benefitted from the use of metatranscriptomics, a method of assessing host-pathogen interactions based on associated gene expression changes (11). The use of metatranscriptomics has been reviewed extensively (12), however, current published methods are based on, or optimisations of, cell culture models as developed in the original methods article (11). The use of metatranscriptomics in natural polymicrobial infections is not as well reported. The first documented use was in relation to the onset of paediatric asthma (13), and oral disease (14, 15). However, its application to Bovine Digital Dermatitis (BDD) (16), which has a similar clinical presentation and bacteria associated with footrot (17–20) highlighted its suitability to further our understanding of the inter-cellular microbial populations associated with

98 agricultural diseases. Utilising this experimental design, we have been able to
99 determine the bacterial populations on the surface of the interdigital skin and within
100 the deeper infected tissue, identify the differential expression of the host transcripts
101 and elucidate interactions between the host and bacteria.

102 ## Results

103 ### *Sequence data*

104 Foot swabs and whole thickness skin biopsies were collected from sheep post
105 slaughter that had at least one apparently healthy foot (n=13) and one with signs of
106 footrot (n=13) to obtain matching samples from the same sheep. After quality filtering
107 there was an average of 8.7 million discordant ovine reads per sample to be used for
108 bacterial taxonomic assignment from the foot biopsies, and 20.8 million discordant
109 ovine reads for the accompanying swabs. All reads had an average phred score of
110 40. Diversity statistics were calculated for each sample after assignment. Using the
111 Shannon indices and calculating an equitability score (natural log of the species
112 richness) representing a maximum diversity, revealed that healthy feet were highly
113 diverse but footrot feet showed a reduction in diversity (Table 1, Fig 1A). The
114 Simpson indices also indicated that there was more diversity in the healthy samples
115 with an average of 0.78 in healthy compared to 0.69 in the footrot biopsies. (Figure
116 1B). This was furthermore reflected in the swabs with an average of 0.94 in the
117 healthy samples compared to 0.77 in footrot (Figure 1). The Shannon index showed
118 a significant difference between the two conditions for both, biopsies ($p=\leq 0.005$) and
119 swabs ($p=\leq 0.05$), whereas only the swabs showed a significant difference for the
120 Simpson index ($p=\leq 0.005$; Figure 1).

121

Table 1 Comparison of average calculated and maximum diversity for each condition. Demonstrating the overall reduction in bacterial community diversity for footrot affected individuals when compared to the calculated maximum diversity expected from the data.

Condition	Biopsy Equitability	Biopsy Shannon	Swab Equitability	Swab Shannon
Healthy	3.9	2.5	7.1	5.0
Footrot	3.3	1.9	7.1	3.2

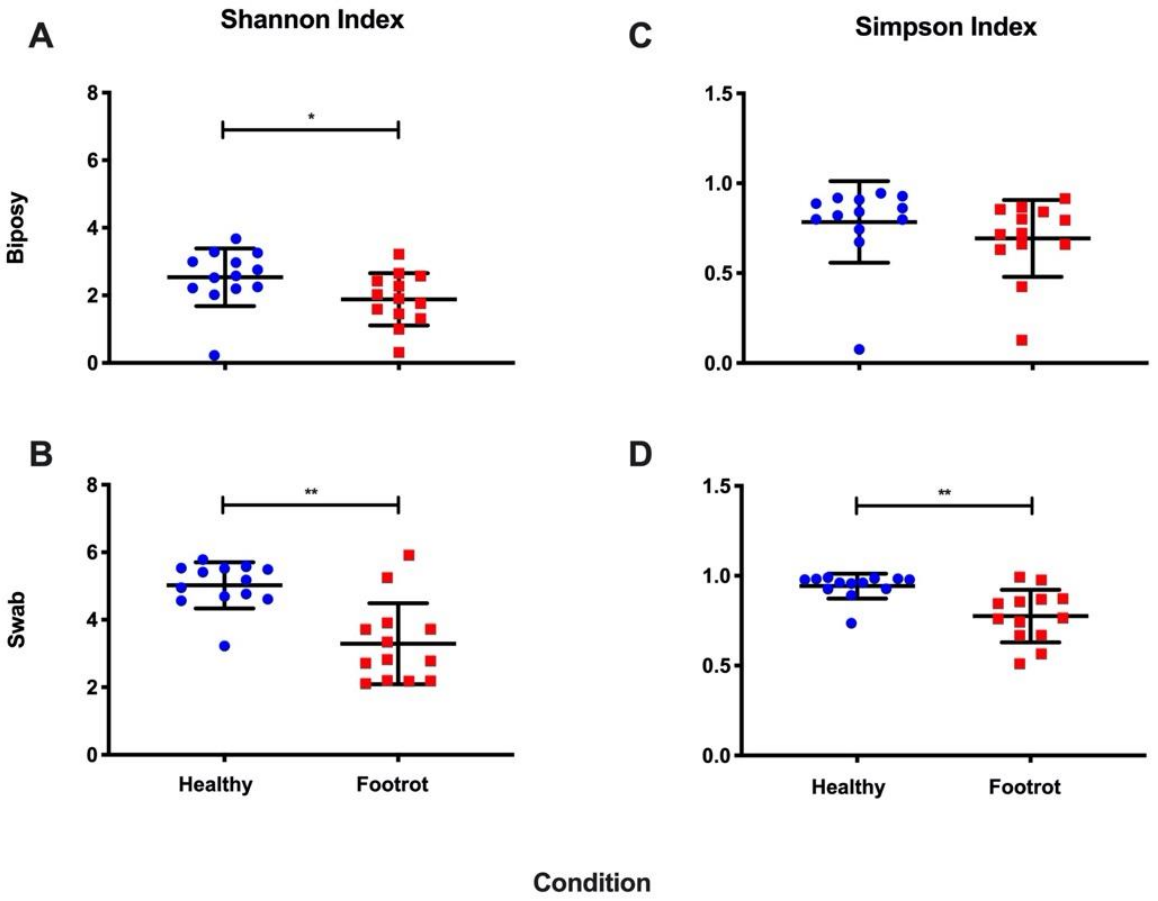

Figure 1 Diversity statistics for the biopsy and swab samples. A) Shannon Index of biopsy samples, B) Shannon Index of swab samples, C) Simpson Index of biopsy samples, D) Simpson index of swab samples. Significant decreases were observed from footrot affected samples, for swabs using both Shannon and Simpson indices. A significant decrease in footrot affected samples was only observed for biopsies using the Shannon index. Statistical significance calculated using Mann Whitney U (* p=0.05, ** p=0.005, *** p=0.0005).

Bacterial community

Differences in abundance calculated between the two conditions were identified as samples having a >2 log fold change, with an FDR (Benjamini-Hochberg) corrected p-value <0.05 and where average counts had a difference greater than 10 (full taxonomic assignments are available in Supplementary Table 1 for swabs and Supplementary Table 2 for biopsies). In swabs, 20 species of bacteria were found in significantly increased abundance in footrot samples. These included *T. pedis, T. denticola, D. nodosus*, and *F. necrophorum,* all known to cause various foot diseases in sheep. Among the bacterial species found in significantly reduced abundance in footrot samples were ten species of *Staphylococcus* spp., *Bacillus licheniformis*, *Parageobacillus thermoglucosidasius* and *Nocardiopsis alba*. All differential abundance data for the swabs are available in Supplementary Table 3.

Applying the same criteria to biopsies, three species of bacteria were found in differential abundance between the two conditions, namely *D. nodosus, Mycoplasma fermentans (M. fermentans)* and *Porphyromonas asaccharolytica (P. asaccharolytica). D. nodosus* had the most significant increase in footrot biopsies with a log-fold change increase of 7.0 (p=1.89E-06), *M. fermentans* had a log-fold change of 6.2 (p=2.59E-05) whilst *P. asaccharolytica* had a log-fold increase of 3.5 (p=0.018). No species were found to be significantly decreased between the two conditions in the biopsies (all differential abundance data for the biopsies are available in Supplementary Table 4). Although some archaea were identified in both biopsy and swab samples, none were significantly more or less abundant in footrot affected feet compared to healthy feet.

As short read sequencing has limitations in identifying bacteria to species level, the most significantly increased abundant bacteria in footrot affected tissues were confirmed to be *D. nodosus*, *M. fermentans* and *P. asaccharolytica,* by specific qPCR, species specific PCR and PCR followed by sequencing, respectively. In addition, *F. nucleatum* was identified as the only *Fusobacterium* species, however qPCR demonstrated this as misidentification and *F. necrophorum* was present as expected.

Comparative analysis of in tissue and surface bacterial communities

The taxonomic assignments from both, swab and biopsy data, were tested to ascertain whether a clear relationship existed between taxonomic assignments for the same sheep using both the correlation and similarity hypothesis tests outlined in the methods section. Under the null hypothesis for the correlation test, there was no correlation between swab and tissue samples. A p-value of 0.0301 was obtained, providing strong evidence of a relationship. However, it should be noted that this is evidence of a relationship in the presence of bacterial species between biopsy and swab samples rather than them containing the same species.

To test the latter claim, the similarity test from the methods section was used. Here, the null hypothesis was that biopsy and swab samples reveal the presence of the same bacteria. This test produced a conservative p-value of < 10^-5, providing over overwhelming evidence that swab and biopsy samples from the same sheep do not contain the same species of bacteria. Specifically, two random biopsy samples will have more species in common than a swab and biopsy from the same sheep.

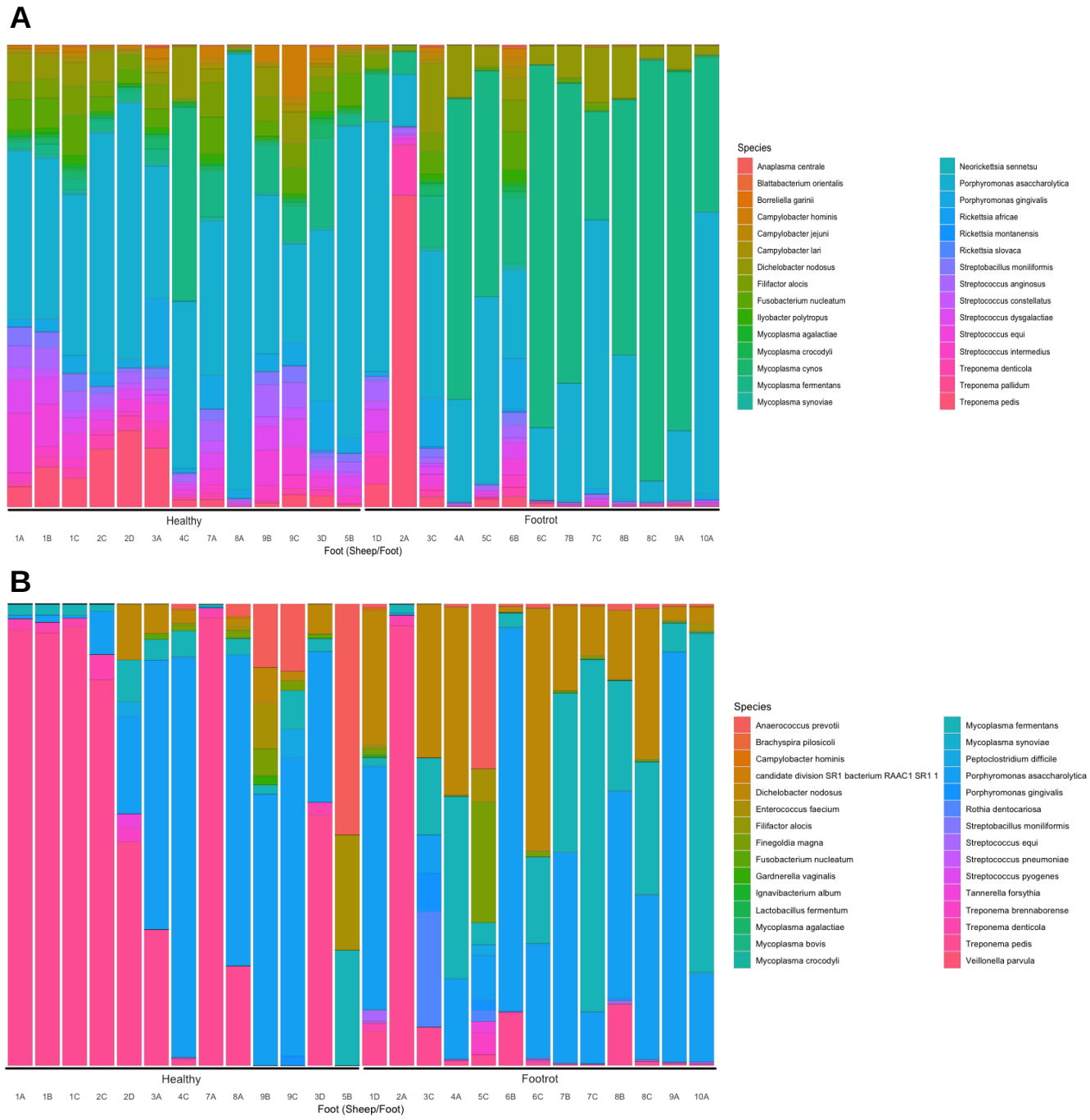

Figure 2 Species of bacteria identified as increased in abundance in footrot affected feet when compared to healthy feet. A) Shows the top 30 species of bacteria in swab samples and B) Shows the top 30 species of bacteria in biopsy samples.

Differential expression of pro-inflammatory mediators in healthy versus footrot affected interdigital skin.

Among the transcripts that showed increased expression in footrot-affected interdigital skin were a large number of proteins important for barrier function. These included proteins involved in collagen production and collagen binding (Procollagen C-endopeptidase enhancer 2 [PCOLCE2], Collagen Type VI alpha 6 chain, Collagen Type XXIII alpha 1 chain and keratocan/lumican [collagen-binding leucine-rich proteoglycans widely distributed in interstitial connective tissues]; cell-cell adhesion (cadherin[CDH]3, CDH19,pro[P]CDH10); maintenance of cell junctions (GJB4) and long chain fatty acid synthesis (fatty acid elongase [ELOVL]7, ELOVL3, acyl-CoA synthetase bubblegum family member [ACSBG]1), and acyl-CoA wax alcohol acyltransferase [AWAT]1). In addition, transcripts involved in immunosurveillance such as scavenger receptors SCARA5 and SSC5D were more highly expressed in footrot affected samples (see Table 2 for top 25 transcripts, Supplementary Table 5 for all transcripts). In contrast, transcripts that showed lower expression compared to healthy interdigital skin include cytokines involved in wound-healing (IL-19, IL-20) and keratinocyte proliferation/differentiation (IL-6 and leukaemia inhibitory factor [LIF]), epithelial cell-derived chemokines that recruit monocytes (CCL2), lymphocytes (CCL20) and neutrophils (CXCL1, CXCL8) and prostaglandin-endoperoxide synthase 2 (PGE2/COX2), which is also involved in skin wound healing. Another group of significantly decreased transcripts include matrix metalloproteases (MMP1, MMP3, MMP9, MMP13, MMP20, (tenacin C) TNC, TIMP1) and their regulators (SERPINE1, ADAMTS4, ADAMTS16) associated with chronic wounds and collagen turnover (see Table 3 for top 25 transcripts, Supplementary Table 5 for all transcripts).

Table 2: Top 25 differentially higher expressed genes in footrot affected skin when compared to healthy skin

Gene name	Description	β-value	Standard error	q-value
ELOVL7	ELOVL fatty acid elongase 7	2.812237	0.884427	0.035516
MNT	MAX network transcriptional repressor	2.415885	0.773256	0.038156
FRAS1	Fraser extracellular matrix complex subunit 1	2.358302	0.738887	0.034774
CA6	carbonic anhydrase 6	2.273248	0.686033	0.029014
ATP13A4	ATPase 13A4	2.261712	0.648362	0.023149
PNPLA5	patatin like phospholipase domain containing 5	2.230351	0.627058	0.021215
ELOVL3	ELOVL fatty acid elongase 3	2.070317	0.598268	0.02425
STMN2	stathmin 2	2.021979	0.464736	0.007856
NOS1	nitric oxide synthase 1	2.004654	0.546986	0.018297
ACSBG1	acyl-CoA synthetase bubblegum family member 1	1.933404	0.590342	0.030742
AWAT1	acyl-CoA wax alcohol acyltransferase 1	1.849357	0.543633	0.02594
CCL26	C-C motif chemokine ligand 26	1.842727	0.621591	0.046882
CCDC155	coiled-coil domain containing 155	1.791928	0.584831	0.041351
PI16	peptidase inhibitor 16	1.765247	0.400402	0.007477
FAR2	fatty acyl-CoA reductase 2	1.711846	0.519782	0.02993
PTX4	pentraxin 4	1.681009	0.336588	0.004979
LRRC36	leucine rich repeat containing 36	1.669794	0.465845	0.020504
AGTR1	angiotensin II receptor type 1	1.661825	0.442673	0.016379
GALNT8	polypeptide N-acetylgalactosaminyltransferase 8	1.631845	0.457915	0.020974
CYP2F1	cytochrome P450 family 2 subfamily F member 1	1.55567	0.44436	0.022765
TOGARAM2	TOG array regulator of axonemal microtubules 2	1.530427	0.48021	0.035066
DNASE1L2	deoxyribonuclease 1 like 2	1.515543	0.406144	0.0169
FAM221A	family with sequence similarity 221 member A	1.506933	0.378682	0.01257
AQP9	aquaporin 9	1.506146	0.384521	0.013256
DGAT2L6	diacylglycerol O-acyltransferase 2 like 6	1.505104	0.480771	0.03797

qval: FDR adjusted p-value using Benjamini-Hochberg; β-value: bias estimator analogous to fold change

Table 3: Top 25 lower expressed genes in footrot affected interdigital skin compared to healthy skin

Gene name	Description	β-value	Standard error	q-value
IL-19	interleukin 19	-2.96775	0.804409	0.017781
PTGS2	prostaglandin-endoperoxide synthase 2 (PGE2/COX2)	-2.8683	0.75813	0.015736
MMP3	matrix metallopeptidase 3	-2.71059	0.616087	0.007597
IL-6	interleukin-6 precursor	-2.4267	0.568937	0.008635
IL-20	interleukin 20	-2.30205	0.758643	0.04305
A2ML1	alpha-2-macroglobulin like 1	-2.23879	0.765254	0.049443
CCL20	C-C motif chemokine ligand 20	-2.18479	0.501858	0.007856
CXCL8	Interleukin-8	-2.10659	0.685411	0.040981
SLPI	antileukoproteinase precursor	-2.04964	0.672506	0.042275
MGAM	maltase-glucoamylase	-2.02022	0.568845	0.021334
MARCKSL1	MARCKS like 1	-1.95955	0.631205	0.039119
MEFV	MEFV, pyrin innate immunity regulator	-1.90552	0.514121	0.017474
MMP13*	matrix metallopeptidase 13	-1.83676	0.523263	0.022523
ADAMTS16	ADAM metallopeptidase with thrombospondin type 1 motif 16	-1.80019	0.479709	0.016379
ACOD1	aconitate decarboxylase 1	-1.68652	0.563289	0.045291
PTX3	pentraxin 3	-1.66311	0.446328	0.016904
MMP13*	matrix metallopeptidase 13	-1.65481	0.561768	0.048097
ADAMTS4	ADAM metallopeptidase with thrombospondin type 1 motif 4	-1.59355	0.394111	0.011418
MMP1	matrix metallopeptidase 1	-1.55518	0.37913	0.01037
FOSL1	FOS like 1, AP-1 transcription factor subunit	-1.51685	0.383897	0.012932
MGAT3	mannosyl (beta-1,4-)-glycoprotein beta-1,4-N-acetylglucosaminyltransferase	-1.46074	0.377507	0.014131
CCL2	C-C motif chemokine ligand 2	-1.40425	0.325691	0.008232
CSF3	colony stimulating factor 3	-1.4015	0.473053	0.047061
PLAUR	urokinase plasminogen activator surface receptor precursor	-1.36363	0.322566	0.009128

qval: FDR adjusted p-value using Benjamini-Hochberg; β-value: bias estimator analogous to fold change

*Splice variants

Biological process enrichment

Using BCCC biclustering and associated GO biological processes, the genes and conditions grouped into a total of 32 clusters. There were 2531 genes over 20 samples that clustered showing upregulated biological processes including significant positive regulation. The top 15 were positive regulation of transcription (n=106, p=2.94e-26), protein folding (n=34, p=3.5e-21), regulation of DNA templated transcription (n=121, p=4.51e-21), metabolic process (n=61, p=1.44e-18), DNA templated transcription (n=63, p=1.48-18), rRNA processing (n=20, p=9.12e-15), protein transport (n=32, p=2.08e-13), ribosome biogenesis (n=17, p=2.20e-13), osteoblast differentiation (n=24, p=4.01e-12), transcription from RNA polymerase II promotor (n=49, p=5.84e-12), negative regulation of transcript from RNA polymerase II promotor (n=63, p=7.75e-12), negative regulation of apoptotic process (n=46, p=1.91e-11), positive regulation of telomerase RNA localisation to cajal body (n=10, p9.34e-11), proteolysis (n=63, p=1.65e-10) and translational initiation (n=16, p=1.74e-10).

There were 541 genes over 17 samples that clustered showing significant downregulation of biological process in footrot affected samples. Cluster one showed a decrease in epidermis development (n=17, p=2.3e-06), multicellular organismal water homeostasis (n=8, p=1.8e-05), peptidoglycan catabolic processes (n=4, p=4.6e-05), antimicrobial humoral response (n=7, p=9.6e-05), tissue development (n=41, p=1.1e-04), monovalent inorganic cation homeostasis (n=8, p=8.2e-4), defence response to bacteria (n=11, p=8.2e-04), fatty acid metabolic processes (n=12, p=1.3e-03), polyol transport (n=3, p=2.7e-03), skin development (n=11, p=2.7e-03), water transport (n=4, p=3.4e-03) and regulation of pH (n=6, p=3.4e-03).

Cluster two showed downregulation for neutrophil chemotaxis (n=7, p=4.3-e06), myeloid leukocyte migration (n=9, p=7.2e-06), leukocyte migration (n=11, p=9.8e-06), cell chemotaxis (n=10, p=2.6e-05), defence response (n=19, p=2.8e-05), immune system processes (n=26, p=4.3e-05), chemotaxis (n=12, p=1.2e-04), antimicrobial humoral response (n=5, p=1.2e-04), immune response (n=18, p=1.2e-04) and response to external stimulus (n=23, p=1.5e-04). The third cluster showed downregulation for S-adenosylhomocysteine catabolic process (n=2, p=5.7e-04) alone.

Investigating KEGG pathway enrichment also identified cytokine-cytokine receptor interaction (n=26, p=4.5e-6), IL-17 signalling pathway (n=13, p=7.7e-08), TNF signalling pathway (n=12, p=7.7e-05) to be downregulated in the footrot affected samples. Whilst steroid hormone biosynthesis (n=7, p=2.4e-04) and ribosome biogenesis (n=31, p=4.07e-08) were upregulated.

Putative Host pathogen interactions

The bacterial RNA reads were aligned against the bacterial transcriptomes that were identified as those traditionally associated with ovine foot disease (*D. nodosus, F. necrophorum*, *T. pedis* and *T. denticola*) and those additionally found to be the most differentially abundant in the footrot biopsy samples *(M. fermentans* and *P. asaccharolytica*). These data were then used, along with the host expression data to understand correlations and host and pathogen interactions (Supplementary Table 6).

The interactions were calculated with an FDR adjusted p-value using the Benjamini-Hochberg procedure. Due to the stringency of this multiple test adjustment, no

279 significance was determined. However, the raw p-values were low (in some cases <
280 0.00005), therefore these data were investigated further but only as an indicative
281 positive bacteria/gene correlation. Based on a raw p-value of <0.00005 there were
282 four sheep transcripts that were associated with five *D. nodosus* genes (Table 4).
283 From *D. nodosus* aminoacyl-histidine dipeptidase, acidic extracellular subtilisin-like
284 protease precursor (AprV5), outer membrane protein 1E, Bacterial extracellular
285 solute-binding protein and aminoacyl-histidine dipeptidase were identified to correlate
286 with small nucleolar RNA, C/D box, U6 spliceosomal RNA, synapsin and U6
287 spliceosomal RNA from *Ovis aries*. There were more correlations between *M.*
288 *fermentans* and *Ovis aries* with a total of 15 bacterial transcripts associated with four
289 host transcripts where raw p=0.0005. The bacterial transcripts were shown to be
290 overwhelmingly responsible for cellular transport on both the host and pathogen side.
291 There were a further three bacterial and sheep interactions in *T. pedis* (p=0.00005)
292 which suggested the bacterial flagellin and host membrane protein, and a bacterial
293 hypothetical protein and putative lipoprotein correlates with a sheep miRNA (Table
294 4).
295
296 The correlations between the sheep transcripts and the bacterial transcripts from *F.*
297 *necrophorum*, *P. asaccharolytica* and *T. denticola* had raw p-values of <0.0005,
298 <0.001 and <0.004, respectively. Although low, p-values with the number of tests
299 being performed they were not investigated any further (full data is available in
300 Supplementary Table 6).
301
302

303 **Table 4. Correlations between bacterial and *host* gene expression.**

Bacterial Species	Protein Accession	Function	*Ovis aries* Transcript accession	Function	p-value
D. nodosus	ABQ13122.1	aminoacyl-histidine dipeptidase	ENSOART00000026163	small nucleolar RNA, C/D box	1.66E-05
D. nodosus	ABQ13667.1	acidic extracellular subtilisin-like protease precursor (AprV5)	ENSOART00000023789	U6 spliceosomal RNA	7.10E-05
D. nodosus	ABQ13351.1	outer membrane protein 1E	ENSOART00000014155	synapsin	7.49E-05
D. nodosus	ABQ13881.1	Bacterial extracellular solute-binding protein			7.49E-05
D. nodosus	ABQ13122.1	aminoacyl-histidine dipeptidase	ENSOART00000023789	U6 spliceosomal RNA	7.49E-05
M. fermentans	WP_013526775.1	Protein translocase subunit	ENSOART00000015973	Pro-platelet basic protein	2.88E-05
M. fermentans	WP_013526734.1	Putative Oligopeptide ABC transporter, ATP-binding protein	ENSOART00000022767	Novel Transcript	4.71E-05
M. fermentans	WP_013526734.1	DNA-directed RNA polymerase subunit beta	ENSOART00000013696	Potassium voltage-gated channel	7.04E-05
M. fermentans	WP_013526778.1	ATP synthase subunit beta	ENSOART00000017736	Novel Transcript	7.04E-05
M. fermentans	ADV34079.1	MgpA like protein	ENSOART00000013889	CXXC Type Zinc Finger 1 CPG Binding PHD Finger	9.28E-05
M. fermentans	WP_013354336.1	bifunctional oligoribonuclease/PAP phosphatase			9.28E-05
M. fermentans	WP_013526633.1	Adenine phosphoribosyltransferase			9.28E-05
M. fermentans	ADV34286.1	Oligopeptide ABC transporter permease protein			9.28E-05
M. fermentans	WP_013354483.1	ABC transporter permease			9.28E-05
M. fermentans	WP_013354556.1	sugar ABC transporter permease			9.28E-05
M. fermentans	ADV34629.1	NADPH flavin oxidoreductase			9.28E-05
M. fermentans	WP_013354747.1	nitroreductase family protein			9.28E-05
M. fermentans	ADV34954.1	Transcription antitermination protein			9.28E-05
M. fermentans	WP_013527166.1	ABC transporter ATP-binding protein			9.28E-05
M. fermentans	WP_013527168.1	ABC transporter permease			2.88E-05
T. pedis	WP_024465740.1	Flagellin	ENSOART00000022912	Novel Membrane Protein	5.38E-05
T. pedis	WP_051150643.1	Hypothetical Protein	ENSOART00000026139	ncRNA (MiRNA)	5.47E-05
T. pedis	AGT42887.1	Putative Lipoprotein			5.47E-05

304

305 **Collagen composition differs in the dermis of healthy and footrot tissues**

306 Since collagen composition changes in scar tissue formation, picrosirius stained
307 tissue sections were used to differentiate collagen type I and III from each other and
308 other collagen types. To investigate whether there were any differences in the
309 collagen composition of the dermis, the proportions of type I, type III, non-
310 differentiated and total collagen were calculated (Fig 4). The proportions of total and
311 type I collagen were significantly increased in the dermis of footrot samples
312 compared to healthy samples ($p=0.04$ and 0.042, respectively, Fig 4 A, D). The
313 proportions of non-differentiated and type III collagen were not significantly different
314 in the dermis layers of healthy and footrot-affected tissues (Fig 4, B-C).

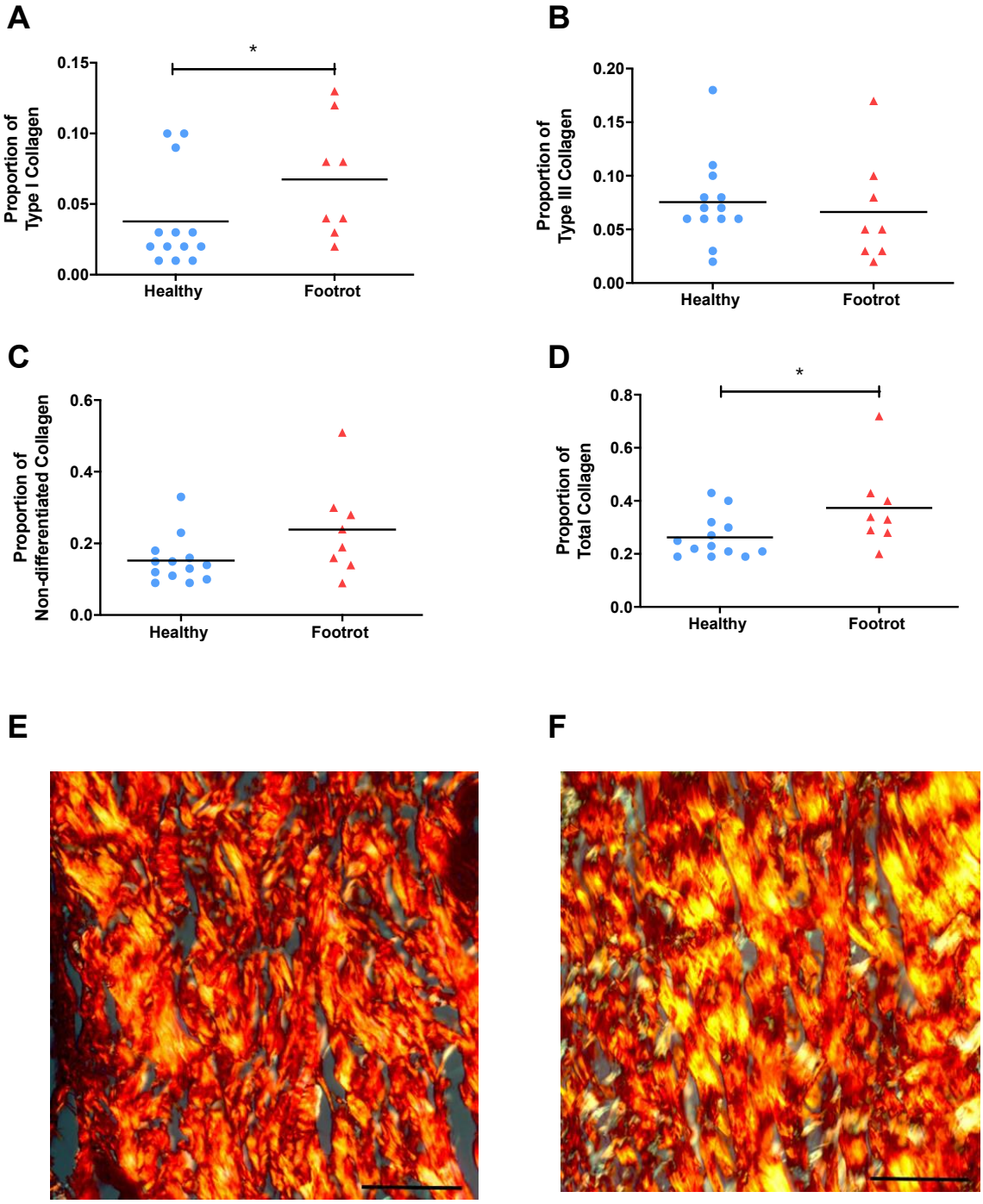

Figure 4: Collagen expression in healthy and footrot ovine interdigital skin dermis. Picrosirius histological staining was used to differentiate and quantify collagens in healthy (n=13) and footrot (n=8) samples. Proportions of type I collagen (A), type III collagen (B), undifferentiated collagens (C) and total proportion of collagen (D). Representative photomicrographs showing picrosirius staining under phase microscopy from healthy (E) and footrot (F) samples, type I collagen stained yellow, type III collagen stained green, undifferentiated collagen stained red. Scale bars represent 50µm. Significance is designated by asterisk on a straight line with the T-test result defined as * = $p \leq 0.05$.

Discussion

D. nodosus, was established as the causative bacterium of ovine footrot in the 1940's, and it has long been accepted that *F. necrophorum* plays a role in the disease aetiology (4). However, in our work we have identified additional common core species that are also associated with footrot lesions (*M. fermentans* and *P. asaccharolytica*) and we have shown putative interactions with the molecular host defence systems during infection in bacterial species identified as highly abundant in footrot and even without a significant difference in abundance between healthy and footrot affected such as *T. pedis*. Using paired biopsies collected from footrot affected sheep at point of slaughter we were able to comprehensively show that skin swabs are a poor proxy for identifying what bacteria are present in the tissue. This is potentially due to the bacterial contamination present from environmental sources such as faeces and soil collected during transport and grazing. However, we have shown that biopsies provide an intradermal approach to reproducibly assess differences between individual animals in an invasive infection like footrot.

The bacterial community structure of footrot

Previous studies have shown the ovine interdigital bacterial community structure using 16S rDNA, with predominant bacterial genera identified as *Mycoplasma spp, Corynebacterium spp, Psychobacter spp, Treponema spp, Staphylococcus spp, Peptostreptococcus spp* and *Dichelobacter spp* (6, 7). The results from this study are highly congruent with what has previously been identified, however due to the greater taxonomic sensitivity afforded by metagenomics and metatranscriptomics we have been able to classify those bacterial genera to a species level. Those with differential abundance associated with footrot found on the skin surface were identified as *T.*

pedis, T. denticola, D. nodosus, and *F. necrophorum.* These species are commonly found with other ovine foot diseases, contagious ovine digital dermatitis (CODD) (21) and interdigital dermatitis (ID) (7) and the bovine foot disease bovine digital dermatitis (BDD) (18). The species with differential abundance associated with footrot intradermally were *D. nodosus, M. fermentans* and *P. asaccharolytica.* Given that *D. nodosus* is a poor pathogen and often requires tissue damage and the presence of other bacteria to infect, it stands to assume *P. asaccharolytica and M. fermentans* may also have an important role in disease susceptibility. These differences between healthy and footrot affected feet also extended beyond presence and absence of species to the overall bacterial diversity, with a significant drop in footrot samples. This reduction in diversity has been mirrored in CODD (21).

The benefits of using metagenomics compared to 16S rDNA studies include that the scope can be extended to incorporate archaeal and DNA virus discovery. In the current study there was a lack of correlation between either and the disease state, however, this may be unsurprising without an enrichment step or optimal DNA extraction to make them specifically more suitable for viral or archaeal identification, resulting in a poor representation for those species identified.

Host response and pathogen interactions

Investigating the host pathogen interactions through correlation analysis has identified some interesting associations which warrant further investigations. The most promising appears to be the association between virulence gene *aprV5* and the *Ovis aries* transcript U6 spliceosomal RNA. This particular non-coding small nuclear RNA (snRNA) is responsible for catalysing the excision of introns and is a major

aspect of post translation modifications, with the ability to alter the structure, function and stability of the translated protein. In the case of infections, some species of bacteria have been implicated in hijacking the host splicing machinery and altering the splicing pattern leading to the perturbation of the host response (22, 23). Despite the lack of knowledge around the mechanism, there is evidence that certain *Listeria, Salmonella* and *Mycobacterium* species have the ability to produce factors that have a direct or indirect impact on the regulation of alternative splicing (23–25). Alternative splicing from the U6 spliceosomal RNA can interfere with the normal activation of T cell and B lymphocytes and the regulation of the signalling in several TLR's (TLR2, TLR3 and TLR4) (26), which could tie in with certain pathways (monovalent inorganic cation homeostasis, defence response to bacteria, skin development, neutrophil chemotaxis, leukocyte migration, defence response, immune system processes, immune response) which were identified as being downregulated in these data.

The acidic extracellular protease *aprV5 is* associated with the correct cleavage of the other proteases secreted by *D. nodosus,* AprV2 and BprV, to their mature active form (Han et al., 2012). Whereas the closely related AprV2 acidic protease is a known virulence factor responsible for elastase activity and its degradation of the host extra cellular matrix (28), the role of AprV5 in footrot is unclear. The abundance of isolates with *aprV5* has been shown to be around 25% from clinically affected farms and lacks any clear delineation between disease severity (29). However, as viral-mediated proteases have been implicated in the degradation of host small non-coding ribonucleal proteins (snRNP) (30) and other bacteria possess other mechanisms of action on snRNP's it may be an interesting focus of future studies.

401 ***Sheep interdigital skin microbiota and scar tissue formation in footrot***

402 The host response to the skin microbiota has to be carefully regulated as innocuous
403 microbes and the host surveillance at epithelial barriers are in constant close
404 proximity. In healthy tissues bacteria are located predominantly in the epidermis
405 while tissue damage and invasive bacteria such as *D. nodosus* allow access of
406 bacteria into deeper dermal tissue layers (10). The ovine host response to footrot
407 demonstrated through differential expression of a range of transcripts involved in
408 proinflammatory mediation (cytokines; IL-19, IL-20, IL-6, LIF, chemokines; CCL2,
409 CCL20, CXCL1, CXCL8 and prostaglandin-endoperoxide synthase 2; PGE2/COX2),
410 of matrix metalloproteases (MMP1, MMP3, MMP9, MMP13, TNC, TIMP1) and
411 interestingly their regulators (SERPINE1, ADAMTS4, ADAMTS16) during footrot, all
412 of which are associated with wound healing, collagen turnover and scar tissue
413 formation. Collagen I was detected significantly more in diseased dermis than in non-
414 infected dermal tissue leading to the conclusion that infection or co-infection clearly
415 indicates current, or ongoing, scar formation in the dermis.

416

417 The process of second intention wound healing with scar formation is classically
418 divided into three main overlapping phases: inflammation, proliferation, and
419 remodelling. Localised inflammation is the first response to any breach of
420 haemostasis with the initiation of cytokine and chemokine production leading to
421 neutrophil and macrophage recruitment to the site of inflammation (31). The
422 cytokines and chemokines IL-6, CCL2, CXCL1, CXCL8 identified as differentially
423 expressed in response to footrot, are associated with acute inflammation in response
424 to tissue injury (31, 32). In normal skin wound healing, the inflammation usually lasts
425 for 2–5 days and ceases once the harmful stimuli have been removed. The IL-20

cytokine family (IL-19, IL-20, IL-22, IL-24, IL-26) contribute to various stages of this wound healing process: they are primarily secreted by infiltrating innate immune cells and lymphocytes shortly after an injury. Initially released by infiltrating macrophages, they preferentially stimulate keratinocytes to secrete antimicrobial peptides and chemokines, in order to reduce infection and accelerate inflammation, and to produce increased levels of vascular endothelial growth factor A (VEGFA), which in turn promotes angiogenesis. IL- 20 subfamily cytokines directly stimulate keratinocyte proliferation and migration, and indirectly support the proliferation of keratinocytes by enhancing the production of epidermal growth factor (EGF) and keratinocyte growth factor (KGF) (33). Surprisingly, we observed significantly reduced expressed IL-19 and IL-20 transcripts in footrot samples. This was accompanied by reduced expression of secretory leucocyte protease inhibitor 1 (SLP1), a protein essential for optimal wound healing due to its antimicrobial and anti-inflammatory properties (34). Macrophages, initially producing pro-inflammatory mediators, transition in response to local immune signals to an anti-inflammatory phenotype. This promotes the resolution of inflammation and a transition to the proliferation phase of second intentiaon wound healing focusing on re-epithelialisation through migration and proliferations of keratinocytes, deposition of type III collagen, and angiogenesis (31). Matrix metalloproteases (MMPs) are crucial to this phase as extracellular matrix degradation and deposition is essential for wound re-epithelialisation and also during tissue remodelling. MMP expression and activity are tightly controlled during wound healing, at the expression levels and through endogenous tissue inhibitors of metallo proteases (TIMPs); specific MMPs are confined to particular locations in the wound and to specific stages of wound repair (35). MMP-1, MMP-3, and MMP-9 are the major chemokine regulators during wound healing, degrading chemokines by

proteolysis and promoting the transition to the proliferation phase. MMPs-1, 8, 9 and 13 are transiently upregulated to remodel the fibrin clot and replacing it with new extracellular matrix. In addition, they are fundamentally stimulating the migration of keratinocytes into the wound bed. During re-epithelialisation, keratinocytes migrate from the surrounding epithelium and proliferate to achieve wound closure**.** This is accompanied by a decreased expression of pro-migratory MMPs (MMP-1 & 2) and an increased tissue remodelling MMP-3 expression (35, 36).

The dysregulation of MMPs leads to prolonged inflammation and delayed wound healing (37). In footrot affected tissues we observed differential expression of the collagenases MMP-1 and 13, the gelatinase MMP-9 and the stromalysin MMP-3. It is well established that high levels of MMP-1 lead to defective re-epithelialisation, with MMP-13, expressed deeper in the tissues, leading to granulation tissue formation (37). Increased MMP-9 levels are consistent with chronic wounds, leading to the reduced expression of the growth factors required for the healing process while prolonging the inflammatory phase (37). The stromalysin MMP-3 is expressed by proliferating keratinocytes at the distal end of the wound and is essential for wound healing (37). However, we observed reduced expression compared to uninfected interdigital skin tissue, which would impact on the ability of infected interdigital skin tissue to heal. Long chain fatty acids and collagens are essential for skin barrier function (36, 38). The increase in expression of fatty acid elongases (ELOVL]7, ELOVL3, ACSBG1) and of proteins involved in collagen production and collagen binding in response to footrot suggests some level of skin regeneration is ongoing.

One of the bacteria significantly increased in abundance on footrot-infected lesions, *M fermentans*, might affect the ability of host skin cells to respond to bacterial

476 infection. Chronic infections of monocytes and macrophages with intracellular low
477 pathogenic Mycoplasma spp. of have been shown to impair their inflammatory
478 response to live bacteria and bacterial products (39, 40). That we see higher
479 transcript levels of outwardly healthy interdigital skin is in contrast to the lack of
480 detection of MMP RNA in healthy human or murine skin (41). However, this is
481 consistent with a marked expression of the inflammatory cytokines/chemokine IL1β,
482 IL6 and CXCL8 in outwardly healthy ovine interdigital skin, which might be due to the
483 constant environmental changes and pressures impacting on interdigital skin or might
484 be associated with subclinical disease that may have developed into ID and footrot in
485 the future (7). During the remodelling phase of scar tissue formation, initially
486 deposited collagen-III molecules are gradually replaced by type I collagen and their
487 orientation becomes more organised (36). Mature cutaneous scars consist of 80-90%
488 type I collagen arranged in parallel bundles (42). This particular orientation as well as
489 less pronounced or missing rete ridges weaken the strength of the scar tissue
490 compared to normal skin in humans to only 70-80% (36). This renders the tissue
491 more susceptible to injury and trauma which are suspected predisposing factors of
492 footrot. The latter might also contribute to the frequently observed relapses and
493 underlines the not only polymicrobial but rather multifactorial aetiology of footrot. For
494 BDD a dysfunctional skin barrier and disturbed tissue integrity is hypothesised to be
495 an essential prerequisite for infection altogether since experimental disease models
496 without skin maceration prior to infection fail to mirror naturally occurring BDD lesions
497 appropriately (43).
498
499 Currently there is conflicting evidence of the impact of the microbiome on wound
500 healing, with some evidence of host commensal interactions promoting wound

healing while colonisation of pathogenic bacteria may invade deeper into tissues or lead to chronic infections and biofilm formation (44, 45). In the context of footrot, we identified another bacterial species in addition to *D. nodosus* that is associated with footrot and also known to be a synergistic wound pathogen, *P. asaccharolytica*. When present in combination with anaerobic and aerobic bacteria such as *Prevotella melaninogenicus*, *Peptostreptococcus micro* and *Klebsiella pneumoniae, P. asacharolytica* exacerbates the disease process (46–48). While antibiotic injections will affect indiscriminately on commensal and pathogenic bacteria, the effectiveness of parenteral antibiotics in footrot demonstrate their high impact on the pathogenic bacteria leading to swift recovery in most cases (49). Interestingly, resistance genes against tetracycline, the most commonly used antibiotic against footrot have so far not been identified in *D. nodosus* genome sequences, suggesting that the antibiotic treatment mainly affects other microbes of that polymicrobial infection enabling host immune system to eliminate *D. nodosus*.

Conclusion

Ovine footrot is a complex polymicrobial disease and there is a clear need to further elucidate the intricate host microbial interactions. We aimed to investigate the host response as well as the microbial taxa in tissues and their intra-tissue expression levels using metatranscriptomics in naturally infected tissues. It is well published that skin damage is required to allow *D. nodosus* infection to establish (2, 50). As expected, the host response in footrot is characterized by differential expression of proteins with roles in wound healing and chronic wounds. As in the absence of *D. nodosus*, interdigital dermatitis resolves, the presence of *D. nodosus* may be essential to allow the establishment of the microbes associated with under running footrot, including *P. asaccharolytica*. In these later stages of disease, the presence of

those bacteria, such as *M. fermentans*, may contribute to a dampening of the immune response unable to remove the invading bacterial pathogens leading to chronic infection.

Materials and Methods

Sample collection

Sheep were assessed post slaughter for foot health. Any individual animals showing signs of footrot were selected for sample collection. Debris was removed from all the feet and cleaned using purified water. Sterile nylon flock swabs (E-swabs 480CE, Copan U.S.A.) were taken from the interdigital space and stored in liquid Amies media at 5°C overnight. The foot was then washed with a chlorohexidine solution (National Veterinary Services, U.K.). Any hair was removed from the feet with scissors, prior to the collection of an 8mm biopsy using a punch (National Veterinary Services, U.K.). Biopsies were placed in RNALater (Sigma Aldrich, U.K.), stored at 5°C overnight before being frozen at -80°C.

DNA Extraction from swabs

The interdigital space swabs were placed on a MixMate (ThermoFisher, U.K.) for 5 minutes at 800rpm to thoroughly disperse the bacteria in the amies solution from the swab. The liquid was transferred into a low-bind 1.5ml tube and centrifuged at 12,000 rpm for 5 minutes. The supernatant was removed, and the pellets were resuspended in 200µl of RNAse-free molecular biology grade water (Thermo Fisher, U.K.) (51). DNA was isolated using the Qiagen Cador Pathogen Mini Kit, following the

manufacturer's guidelines, eluted in 60μl of elution buffer. The DNA samples were quantified using the Qubit 3.0 and dsDNA high sensitivity dye (Qiagen).

RNA Extraction

Biopsies were thawed on ice before being cut into approximately 30mg sections. One section was added to a MACs M tube (Miltenyi Biotech, U.K.) containing 1ml Qiazol (Qiagen, U.K.) and dissociated on a GentleMACs (Miltenyi Biotech, U.K.) using the manufacturers RNA settings. The sample was centrifuged and incubated at room temperature (RT) for 5 minutes before transferring the lysate to a 1.5ml centrifuge tube. Proteinase K (20μl) was added to the sample before being incubated at 56°C for an hour. Chloroform (200μl) was added and shaken vigorously for 15 seconds. The sample was then incubated at RT for 2 minutes before being centrifuged at 12,000xg for 15 minutes at 4°C. The upper aqueous phase was transferred to a fresh 1.5ml centrifuge tube before the addition of 1x volume of 70% ethanol. The sample (up to 700μl) was added to an RNeasy Mini Spin column (Qiagen, U.K.) and centrifuged at RT at 8000xg for 30 seconds. Any remaining sample was also passed through the column. All remaining steps followed the manufactures guidelines with elution in 30μl of RNAse-free molecular biology grade water (Thermo Fisher, U.K.).

Dual RNA Sequencing

The extracted RNA was quantified using the Agilent Bioanalyser RNA Nano 6000 kit. Healthy foot sample RNA with a RIN score of ≥7 and footrot sample RNA with a DV200 >85 was chosen for sequencing. The samples were treated using the RiboZero Gold (epidemiology) ribosomal depletion kit (Illumina, U.S.A.) and prepared for sequencing using Illumina TruSeq library preparation (Illumina, U.S.A.). The

576 samples were sequenced on a HiSeq 3000 using 150bp paired end chemistry (Leeds
577 Institute of Molecular Medicine, sequencing facility) at 6 libraries per lane over 14
578 lanes giving approximately 75 million reads per sample.
579
580 ***Data Analysis***
581 All analysis was carried out using default settings unless stated. Raw reads were
582 analysed for quality and adaptor removal using Skewer (52). An initial step for the
583 RNASeq data consisted of aligning the reads with HISAT2 (53) against the sheep
584 genome (Oar_v3.1, downloaded 21/07/2017) (54) to separate the ovine and potential
585 bacterial transcripts. The sheep reads were then parsed for transcript alignment
586 using Kallisto (55) and the sheep genome (Oar_v3.1, downloaded 21/07/2017) (54).
587 Differential analysis was calculated with Sleuth (56). The differentially expressed
588 genes were imported in R (57) and clustered using BiClust and the Block Correlated
589 Coupled Clustering (58). The reads which did not align to the sheep genome and the
590 metagenomic reads were used as input for taxonomic assignment and bacterial
591 populations were determined with Kraken (59), false positives were identified with
592 KrakenUniq (60) and results were filtered with MAG_TaxaAssigner
593 (https://github.com/shekas3/BinTaxaAssigner).
594
595
596 ***Confirmation of selected bacterial species by PCR or qPCR***
597 Parallel tissue samples from the same foot as for RNA isolation were used. Tissue
598 homogenisation and DNA extractions were performed as described previously using
599 QIAamp Cador kit (Qiagen) (61). The DNA samples were quantified using the Qubit
600 3.0 and dsDNA high sensitivity dye (Qiagen). Bacterial load was quantified using
601 real-time PCR based on 16S rRNA gene for eubacteria (62) and *D. nodosus* (63), *F.*

602 *necrophorum* subspecies necrophorum primers targeted the gyrB gene (51). *M.*
603 *fermentans* sequences were amplified by species specific PCR for 16S rRNA (64)
604 and *P. asaccharolytica* sequences were amplified by PCR (65) followed by
605 sequencing (Eurofins Genomics).
606
607 ***Correlation Testing***
608 Both tests were performed using the same dataset. For each of the samples (biopsy,
609 swab and host), each of the bacteria species were labelled as either present or
610 absent in each sample. A difference score was prescribed if species was present in
611 one of the swab or biopsy samples from a sheep but, not both (i.e., the swab and
612 biopsy gave different results for the presence of the species). If present in both or
613 neither the biopsy nor swab samples for then. A t-test statistic was calculated by
614 taking the sum of all differences across all sheep. To perform the randomisation
615 procedure the labels of the original 52 samples (sheep and sample type) were
616 randomly reassigned and the test statistic recalculated. This procedure was repeated
617 10 000 times, giving randomised test statistics.
618
619 ***Host Pathogen Interactions***
620 To identify putative host pathogen interactions the correlation script PHInder was
621 used (https://github.com/addyblanch/PHInder). Briefly, samples with zero
622 assignments were removed, and a minimum presence value was set to one. A new
623 data matrix was formed and the hypergenometric distribution was calculated using
624 phyper
625 (https://www.rdocumentation.org/packages/stats/versions/3.6.2/topics/Hypergeometri
626 c) and a probability, producing a significance (p) value and adjusted p value.

627 ***Tissue staining, image capture and analysis***

628 Biopsies were processed in ethanol and xylene, mounted in paraffin and 7 μm thick
629 serial sections collected throughout the tissue onto polysilinated microscope slides.
630 The paraffin from each tissue section was melted at 60°C for 5-10min, followed by
631 immersed in xylene twice for 5min each to remove the paraffin. Tissue sections were
632 then rehydrated in 100% ethanol, 90% ethanol, 70 % ethanol and distilled water for
633 5min each. Picrosirius red (PS) stain was used to differentiate and quantify collagen
634 types I, III and undifferentiated collagens using the picrosirius stain kit (Polysciences,
635 Inc., Pennsylvania, USA). The observer was blinded to the sample identification to
636 avoid subconscious bias. Images were captured using a Leica CTR500 microscope
637 (Leica Microsystems, Germany) with or without polarised light. For each sample,
638 three sections approximately 400 μm apart were analysed. At 40x magnification, five
639 non-overlapping photos were taken from each section from the dermis of PS stained
640 sections (330 photomicrographs analysed).
641
642 For 13 healthy and 8 footrot samples, 15 photomicrographs per sample were
643 captured (systematic random sampling) and analysed using Image-Pro Plus (Media
644 Cybernetics, Inc, Pennsylvania, USA) to quantify the area of collagen in each image,
645 with separate measurements for type III (green), type I (yellow) and undifferentiated
646 (red) collagen (315 images analysed in total). Total collagen proportion was
647 calculated as the sum of type III, type I and undifferentiated collagen proportions.
648
649 ***Statistical analysis***
650 The taxonomic count data were analysed for statistically significant differences in R
651 (57) using the edgeR wrapper (66) as part of the Phyloseq package (67). Diversity

652 statistics were calculated using vegan (68) and differences were calculated using
653 Mann-Whitney U tests in Prism 8.01 (GraphPad Software Inc. USA).
654
655 Statistical analyses of histology images were performed on GraphPad Prism version
656 6 for windows. Resulting data were presented as frequencies and percentages and
657 were analysed by student T-test or Kruskal Wallis test, dependent on data
658 distribution. Analysis was taken as significant when $p \leq 0.05$.
659
660 **Author Contributions**
661 AMB and ST developed the idea, designed, and supervised the experiments and
662 alongside SW, CMB, JKM and GE have written the manuscript. AMB completed the
663 bioinformatics analysis. CES, CMB and JKM carried out the lab work, NN performed
664 and analysed bacterial qPCR. CR and CB performed and analysed the collagen
665 assays. LS performed additional statistical and mathematical assessment of the data.
666 All authors have read the manuscript.
667
668 **Ethical Statement**
669 This study was reviewed and approved by the University of Nottingham, School of
670 Veterinary Medicine and Science ethical review committee ERN: 1144 140506 (Non
671 ASPA).
672
673 **Funding**
674 This work was supported by the Biotechnology and Biological Sciences Research
675 Council [grant number BB/M012085/1] (BBSRC) Animal Health Research Club 2014
676 and the University of Nottingham. NB was funded by BBSRC STARs scheme (2017-

677 2019). GE & SRW were also funded by the Scottish Government Rural and
678 Environment Science and Analytical Services (RESAS) GE and SRW also received
679 funding from the European Union's Horizon 2020 research and innovation
680 programme under grant agreement No. 731014 (VetBioNet). The funders had no role
681 in the design of the study, collection, analysis, interpretation of the data nor in the
682 writing of the manuscript.

683

684 **Competing Financial Interests**

685 All the authors state that there is no competing financial interest in the production of
686 this manuscript.

687

688 **Acknowledgements**

689 The authors would like to thank Professor Christoph Mülling for helping facilitate this
690 research collaboration with the Faculty of Veterinary Medicine, Leipzig University.
691 The authors would also like to thank Dr Ian Carr and Ummey Hany at The Leeds
692 Institute for Molecular Medicine Sequencing Facility for all their experimental
693 suggestions and sequencing support.

694

695 **Open Access Data**

696 All sequence data generated for this study is held in the NCBI SRA under the
697 accession number PRJNA725378.

References

1. Kaler J, Medley GF, Grogono-Thomas R, Wellington EM, Calvo-Bado LA, Wassink GJ, King EM, Moore LJ, Russell C, Green LE. 2010. Factors associated with changes of state of foot conformation and lameness in a flock of sheep. Prev Vet Med 97:237–244.

2. Beveridge W. 1941. Foot-rot in sheep : A transmissible disease due to infection with Fusiformis nodosus (n. sp.). Studies on its cause, epidemiology, and control. Bull Counc Sci Ind Res Aust 140:1–58.

3. Beveridge W. 1936. a Study of Spirochaeta Penortha (N.Sp.) Isolated From Foot-Rot in Sheep. Immunol Cell Biol 14:307–318.

4. Egerton JR, Roberts DS, Parsonson I. 1969. The Aetiology and Pathogenesis of ovine Footrot. J Comp Pathol 79:207–217.

5. Roberts DS, Foster WH, Kerry JB, Calder HA. 1972. An alum-treated vaccine for the control of foot-rod in sheep. Vet Rec 91:428–429.

6. Calvo-Bado LA, Oakley BB, Dowd SE, Green LE, Medley GF, Ul-Hassan A, Bateman V, Gaze W, Witcomb L, Grogono-Thomas R, Kaler J, Russell CL, Wellington EM. 2011. Ovine pedomics: the first study of the ovine foot 16S rRNA-based microbiome. ISME J 5:1426–1437.

7. Maboni G, Blanchard A, Frosth S, Stewart C, Emes R, Tötemeyer S. 2017. A distinct bacterial dysbiosis associated skin inflammation in ovine footrot. Sci Rep 7:45220.

8. Ramírez AS, Fleitas JL, Rosales RS, Poveda C, de la Fe C, Andrada M, Castro A, Poveda JB. 2008. A semi-defined medium without serum for small ruminant mycoplasmas. Vet J 178:149–152.

722 9. Juni E, Heym GA. 1986. Psychrobacter immobilis gen. nov., sp. nov.:
723 Genospecies Composed of Gram-Negative, Aerobic, Oxidase-Positive Coccobacilli.
724 Int J Syst Bacteriol 36:388–391.
725 10. Agbaje M, Rutland CS, Maboni G, Blanchard A, Bexon M, Stewart C, Jones MA,
726 Totemeyer S. 2018. Novel inflammatory cell infiltration scoring system to investigate
727 healthy and footrot affected ovine interdigital skin. PeerJ 6:e5097.
728 11. Westermann AJ, Gorski S a., Vogel J. 2012. Dual RNA-seq of pathogen and
729 host. Nat Rev Microbiol 10:618–630.
730 12. Westermann AJ, Barquist L, Vogel J. 2017. Resolving host–pathogen interactions
731 by dual RNA-seq. PLOS Pathog 13:e1006033.
732 13. Pérez-Losada M, Castro-Nallar E, Bendall ML, Freishtat RJ, Crandall KA. 2015.
733 Dual transcriptomic profiling of host and microbiota during health and disease in
734 pediatric asthma. PLoS ONE 10:1–17.
735 14. Nowicki EM, Shroff R, Singleton JA, Renaud DE, Wallace D, Drury J, Zirnheld J,
736 Colleti B, Ellington AD, Lamont RJ, Scott DA, Whiteley M. 2018. Microbiota and
737 Metatranscriptome Changes Accompanying the Onset of Gingivitis. mBio 9:e00575-
738 18.
739 15. Ram-Mohan N, Meyer MM. 2020. Comparative Metatranscriptomics of
740 Periodontitis Supports a Common Polymicrobial Shift in Metabolic Function and
741 Identifies Novel Putative Disease-Associated ncRNAs. Front Microbiol 11:482.
742 16. Marcatili P, Nielsen MW, Sicheritz-Pontén T, Jensen TK, Schafer-Nielsen C,
743 Boye M, Nielsen M, Klitgaard K. 2016. A novel approach to probe host-pathogen
744 interactions of bovine digital dermatitis, a model of a complex polymicrobial infection.
745 BMC Genomics 17:987.

746 17. Bay V, Griffiths B, Carter S, Evans NJ, Lenzi L, Bicalho RC, Oikonomou G. 2018.
747 16S rRNA amplicon sequencing reveals a polymicrobial nature of complicated claw
748 horn disruption lesions and interdigital phlegmon in dairy cattle. Sci Rep 8:1–12.
749 18. Krull AC, Shearer JK, Gorden PJ, Cooper VL, Phillips GJ, Plummer PJ. 2014.
750 Deep Sequencing Analysis Reveals Temporal Microbiota Changes Associated with
751 Development of Bovine Digital Dermatitis. Infect Immun 82:3359–3373.
752 19. Sullivan LE, Clegg SR, Angell JW, Newbrook K, Blowey RW, Carter SD, Bell J,
753 Duncan JS, Grove-White DH, Murray RD, Evans NJ. 2015. High-level association of
754 bovine digital dermatitis treponema spp. with contagious ovine digital dermatitis
755 lesions and presence of fusobacterium necrophorum and dichelobacter nodosus. J
756 Clin Microbiol 53:1628–1638.
757 20. Zinicola M, Higgins H, Lima S, Machado V, Guard C, Bicalho R. 2015. Shotgun
758 metagenomic sequencing reveals functional genes and microbiome associated with
759 bovine digital dermatitis. PLoS ONE 10:1–17.
760 21. Duncan JS, Angell JW, Richards P, Lenzi L, Staton GJ, Grove-White D, Clegg S,
761 Oikonomou G, Carter SD, Evans NJ. 2021. The dysbiosis of ovine foot microbiome
762 during the development and treatment of contagious ovine digital dermatitis. Anim
763 Microbiome 3:19.
764 22. Kalam H, Fontana MF, Kumar D. 2017. Alternate splicing of transcripts shape
765 macrophage response to Mycobacterium tuberculosis infection. PLOS Pathog
766 13:e1006236.
767 23. Pai AA, Baharian G, Pagé Sabourin A, Brinkworth JF, Nédélec Y, Foley JW,
768 Grenier J-C, Siddle KJ, Dumaine A, Yotova V, Johnson ZP, Lanford RE, Burge CB,
769 Barreiro LB. 2016. Widespread Shortening of 3' Untranslated Regions and Increased

770 Exon Inclusion Are Evolutionarily Conserved Features of Innate Immune Responses
771 to Infection. PLOS Genet 12:e1006338.
772 24. Luo Z, Li Z, Chen K, Liu R, Li X, Cao H, Zheng SJ. 2012. Engagement of
773 heterogeneous nuclear ribonucleoprotein M with listeriolysin O induces type I
774 interferon expression and restricts Listeria monocytogenes growth in host cells.
775 Immunobiology 217:972–981.
776 25. Penn BH, Netter Z, Johnson JR, Dollen JV, Jang GM, Johnson T, Ohol YM,
777 Maher C, Bell SL, Geiger K, Golovkine G, Du X, Choi A, Parry T, Mohapatra BC,
778 Storck MD, Band H, Chen C, Jäger S, Shales M, Portnoy DA, Hernandez R, Coscoy
779 L, Cox JS, Krogan NJ. 2018. An Mtb-Human Protein-Protein Interaction Map
780 Identifies a Switch between Host Antiviral and Antibacterial Responses. Mol Cell
781 71:637-648.e5.
782 26. Chauhan K, Kalam H, Dutt R, Kumar D. 2019. RNA Splicing: A New Paradigm in
783 Host–Pathogen Interactions. J Mol Biol 431:1565–1575.
784 27. Han X, Kennan RM, Steer DL, Smith AI, Whisstock JC, Rood JI. 2012. The
785 AprV5 Subtilase Is Required for the Optimal Processing of All Three Extracellular
786 Serine Proteases from Dichelobacter nodosus. PLOS ONE 7:8.
787 28. Kennan RM, Wong W, Dhungyel OP, Han X, Wong D, Parker D, Rosado CJ, Law
788 RHP, McGowan S, Reeve SB, Levina V, Powers GA, Pike RN, Bottomley SP, Smith
789 AI, Marsh I, Whittington RJ, Whisstock JC, Porter CJ, Rood JI. 2010. The Subtilisin-
790 Like Protease AprV2 Is Required for Virulence and Uses a Novel Disulphide-
791 Tethered Exosite to Bind Substrates. PLoS Pathog 6:e1001210.
792 29. Stäuble A, Steiner A, Normand L, Kuhnert P, Frey J. 2014. Molecular genetic
793 analysis of Dichelobacter nodosus proteases AprV2/B2, AprV5/B5 and BprV/B in
794 clinical material from European sheep flocks. Vet Microbiol 168:177–184.

795 30. Álvarez E, Castelló A, Carrasco L, Izquierdo JM. 2013. Poliovirus 2A Protease
796 Triggers a Selective Nucleo-Cytoplasmic Redistribution of Splicing Factors to
797 Regulate Alternative Pre-mRNA Splicing. PLoS ONE 8:e73723.
798 31. Ellis S, Lin EJ, Tartar D. 2018. Immunology of Wound Healing. Curr Dermatol
799 Rep 7:350–358.
800 32. Hua Y, Bergers G. 2019. Tumors vs. Chronic Wounds: An Immune Cell's
801 Perspective. Front Immunol 10:2178.
802 33. Rutz S, Wang X, Ouyang W. 2014. The IL-20 subfamily of cytokines — from host
803 defence to tissue homeostasis. Nat Rev Immunol 14:783–795.
804 34. Ashcroft GS, Lei K, Jin W, Longenecker G, Kulkarni AB, Greenwell-Wild T, Hale-
805 Donze H, McGrady G, Song X-Y, Wahl SM. 2000. Secretory leukocyte protease
806 inhibitor mediates non-redundant functions necessary for normal wound healing. Nat
807 Med 6:1147–1153.
808 35. Caley MP, Martins VLC, O'Toole EA. 2015. Metalloproteinases and Wound
809 Healing. Adv Wound Care 4:225–234.
810 36. Marshall CD, Hu MS, Leavitt T, Barnes LA, Lorenz HP, Longaker MT. 2018.
811 Cutaneous Scarring: Basic Science, Current Treatments, and Future Directions. Adv
812 Wound Care 7:29–45.
813 37. Krishnaswamy VR, Mintz D, Sagi I. 2017. Matrix metalloproteinases: The
814 sculptors of chronic cutaneous wounds. Biochim Biophys Acta BBA - Mol Cell Res
815 1864:2220–2227.
816 38. Uchida Y. 2011. The role of fatty acid elongation in epidermal structure and
817 function. Dermatoendocrinol 3:65–69.
818 39. Nolan TJ, Gadsby NJ, Hellyer TP, Templeton KE, McMullan R, McKenna JP,
819 Rennie J, Robb CT, Walsh TS, Rossi AG, Conway Morris A, Simpson AJ. 2016. Low-

820 pathogenicity Mycoplasma spp. alter human monocyte and macrophage function and
821 are highly prevalent among patients with ventilator-acquired pneumonia. Thorax
822 71:594–600.
823 40. Zakharova E, Grandhi J, Wewers MD, Gavrilin MA. 2010. Mycoplasma
824 Suppression of THP-1 Cell TLR Responses Is Corrected with Antibiotics. PLoS ONE
825 5:e9900.
826 41. McCarty SM, Cochrane CA, Clegg PD, Percival SL. 2012. The role of
827 endogenous and exogenous enzymes in chronic wounds: A focus on the implications
828 of aberrant levels of both host and bacterial proteases in wound healing: Host and
829 bacterial proteases in wound healing. Wound Repair Regen 20:125–136.
830 42. Lawrence WT. 1998. Physiology of the acute wound. Clin Plast Surg 25:321–340.
831 43. Krull AC, Cooper VL, Coatney JW, Shearer JK, Gorden PJ, Plummer PJ. 2016. A
832 Highly Effective Protocol for the Rapid and Consistent Induction of Digital Dermatitis
833 in Holstein Calves. PLOS ONE 11:e0154481.
834 44. Johnson T, Gómez B, McIntyre M, Dubick M, Christy R, Nicholson S, Burmeister
835 D. 2018. The Cutaneous Microbiome and Wounds: New Molecular Targets to
836 Promote Wound Healing. Int J Mol Sci 19:2699.
837 45. Tomic-Canic M, Burgess JL, O'Neill KE, Strbo N, Pastar I. 2020. Skin Microbiota
838 and its Interplay with Wound Healing. Am J Clin Dermatol 21:36–43.
839 46. Bowler PG, Duerden BI, Armstrong DG. 2001. Wound Microbiology and
840 Associated Approaches to Wound Management. CLIN MICROBIOL REV 14:26.
841 47. Mayrand D, McBride BC. 1980. Ecological Relationships of Bacteria Involved in a
842 Simple, Mixed Anaerobic Infection. INFECT IMMUN 27:7.

843 48. Sundqvist GK, Eckerbom MI, Larsson AP, Sjögren UT. 1979. Capacity of
844 anaerobic bacteria from necrotic dental pulps to induce purulent infections. Infect
845 Immun 25:685–693.
846 49. Jordan D, Nicol' H, Jessep' T, Scrivener C. 1996. Factors associated with the
847 effectiveness of antibiotic treatment for ovine virulent footrot 5.
848 50. Graham NPH, Egerton JR. 1968. PATHOGENESIS OF OVINE FOOT-ROT: THE
849 ROLE OF SOME ENVIRONMENTAL FACTORS. Aust Vet J 44:235–240.
850 51. Frosth S, König U, Nyman A-KK, Pringle M, Aspán A, Konig U, Nyman A-KK,
851 Pringle M, Aspan A. 2015. Characterisation of Dichelobacter nodosus and detection
852 of Fusobacterium necrophorum and Treponema spp. in sheep with different clinical
853 manifestations of footrot. Vet Microbiol 179:82–90.
854 52. Jiang H, Lei R, Ding S-W, Zhu S. 2014. Skewer: a fast and accurate adapter
855 trimmer for next-generation sequencing paired-end reads. BMC Bioinformatics
856 15:182.
857 53. Kim D, Langmead B, Salzberg SL. 2015. HISAT: A fast spliced aligner with low
858 memory requirements. Nat Methods 12:357–360.
859 54. Archibald AL, Cockett NE, Dalrymple BP, Faraut T, Kijas JW, Maddox JF,
860 McEwan JC, Hutton Oddy V, Raadsma HW, Wade C, Wang J, Wang W, Xun X.
861 2010. The sheep genome reference sequence: A work in progress. Anim Genet
862 41:449–453.
863 55. Bray NL, Pimentel H, Melsted P, Pachter L. 2016. Near-optimal probabilistic
864 RNA-seq quantification. Nat Biotechnol 34:525–527.
865 56. Pimentel H, Bray NL, Puente S, Melsted P, Pachter L. 2017. Differential analysis
866 of RNA-seq incorporating quantification uncertainty. Nat Methods 14:687–690.

867 57. Ihaka R, Gentleman R. 1996. R: A Language for Data Analysis and Graphics. J
868 Comput Graph Stat 5:299–314.
869 58. Cheng Y, Church GM. 2000. Biclustering of Expression Data. Proc Int Conf Intell
870 Syst Mol Biol 11.
871 59. Wood DE, Salzberg SL. 2014. Kraken: ultrafast metagenomic sequence
872 classification using exact alignments. Genome Biol 15:R46.
873 60. Breitwieser FP, Baker DN, Salzberg SL. 2018. KrakenUniq: confident and fast
874 metagenomics classification using unique k-mer counts. Genome Biol 19:198.
875 61. Maboni G, Frosth S, Aspán A, Tötemeyer S. 2016. Ovine footrot: New insights
876 into bacterial colonisation. Vet Rec 179.
877 62. Strub S, Van Der Ploeg JR, Nuss K, Wyss C, Luginbühl A, Steiner A. 2007.
878 Quantitation of Guggenheimella bovis and treponemes in bovine tissues related to
879 digital dermatitis. FEMS Microbiol Lett 269:48–53.
880 63. Frosth S, Slettemeas JS, Jorgensen HJ, Angen O, Aspan A. 2012. Development
881 and comparison of a real-time PCR assay for detection of Dichelobacter nodosus
882 with culturing and conventional PCR: harmonisation between three laboratories. Acta
883 Vet Scand 54:6.
884 64. Kuppeveld F Van. 1992. Genus-and species-specific identification of
885 mycoplasmas by 16S rRNA amplification. Appl … 58:2606–2615.
886 65. Tran T, Flynn MJ, Chen C, Slots J. 1997. Absence of Porphyromonas
887 asaccharolytica, Bacteroides fragilis and Chlamydia pneumoniae in human
888 subgingival plaque. Oral Microbiol Immunol 12:377–378.
889 66. Robinson M, McCarthy D, Chen Y, Smyth GKG. 2013. edgeR: differential
890 expression analysis of digital gene expression dataUser's Guide. R Man 1–76.

891 67. McMurdie PJ, Holmes S. 2013. phyloseq: an R package for reproducible
892 interactive analysis and graphics of microbiome census data. PLoS One 8:e61217.
893 68. Oksanen J, Blanchet FG, Friendly M, Kindt R, Legendre P, McGlinn D, Minchin
894 PR, O'Hara RB, Simpson GL, Solymos P, Stevens MHH, Szoecs E, Wagner H. 2018.
895 vegan: Community Ecology Package. CRAN R.